International round-robin experiment for angle-resolved light scattering measurement

A. von Finck, T. Herffurth, A. Duparré, S. Schröder, M. Lequime, Myriam Zerrad, S. Liukaityte, C. Amra, S. Achour, M. Chalony, et al.

International Round-Robin Experiment for Angle Resolved Light Scattering Measurement

A. VON FINCK,[1,*] T. HERFFURTH,[1] A. DUPARRÉ,[1] S. SCHRÖDER,[1] M. LEQUIME,[2] M. ZERRAD,[2] S. LIUKAITYTE,[2] C. AMRA,[2] S. ACHOUR,[3] M. CHALONY,[3] Q. KUPERMAN,[3] Y. CORNIL,[3] A. BIALEK,[4] T. GOODMAN,[4] C. GREENWELL,[4] B. GUR,[5] S. BRINKERS,[5] G. OTTER,[5] A. VOSTEEN,[5] J. STOVER,[6] R. VINK,[7] A. DEEP,[7] AND D. DOYLE[7]

[1]*Fraunhofer Institute for Applied Optics and Precision Engineering IOF, A.-Einstein-Str. 7, 07745 Jena, Germany*
[2]*Institute Fresnel, Domaine Universitaire de Saint Jérôme, 13397 Marseille cedex 20, France*
[3]*Light Tec SARL, Pôle d'Activités Hyérois, 1128 Route de Toulon, 83400 Hyères, France*
[4]*National Physical Laboratory, Hampton Rd, Teddington, Middlesex, TW11 0LW, United Kingdom*
[5]*TNO Industrie en techniek, Stieltjesweg 1, 2628 CK Delft, The Netherlands*
[6]The Scatter Work, Inc., 2100 N. Wilmot, Suite 202, Tucson AZ 85712, USA
[7]*European Space Agency ESTEC, Optics Section (TEC-MMO), Keplerlaan 1, PO Box 299, 2200 AG Noordwijk, The Netherlands*
**Corresponding author: alexandervonfinck@web.de*

Received XX Month XXXX; revised XX Month, XXXX; accepted XX Month XXXX; posted XX Month XXXX (Doc. ID XXXXX); published XX Month XXXX

An international round-robin experiment has been conducted to test procedures and methods for the measurement of angle resolved light scattering. ASTM E2387-05 has been used as the main guide, while the experience gained should also contribute to the new ISO standard of angle resolved scattering currently under development (ISO/WD 19986:2016). Seven laboratories from Europe and the USA measured the angle resolved scattering from Al/SiO_2 coated substrates, transparent substrates, volume diffusors, quasi volume diffusors, white calibration standards, and grating samples at laser wavelengths in the UV, VIS and NIR spectrum. Results were sent to Fraunhofer IOF that coordinated the experiments and analyzed the data, while ESA-ESTEC, as the project donor, defined conditions and parameters. Depending mainly on the sample type, overall good to reasonable agreements were observed, with largest deviations at scattering angles very close to the specular beam. Volume diffusor characterization unexpectedly turned out to be challenging. Not all participants provided measurement uncertainty ranges according to GUM, often, a single general scatterometer-related measurement uncertainty value was stated. Although relative instrument measurement uncertainties close to 1% are sometimes claimed, the comparison results did not support these claims for specular scattering samples as mirrors, substrates, or gratings. *© 2017 Optical Society of America*

OCIS codes: *(290.0290) Scattering; (290.5820) Scattering measurements; (120.4800) Optical standards and testing*

http://dx.doi.org/10.1364/AO.99.099999

1. Introduction

The increasingly demanding requirements of optical systems in the recent few years, especially those of space optical systems, have driven light scattering specifications of optical components to the extreme. Light scattering reduces the optical throughput of optical systems, the lateral resolution of imaging optics, the spectral resolution of spectrometer systems, and it increases stray light problems. As a result, light scattering specifications have become one of the most critical performance parameters of high-end optical instruments and components. Testing these important specifications consequently drives demands for reliable measurements.

Light scattering distributions are described by the angle resolved quantities BSDF (Bidirectional Scattering Distribution Function) or ARS (Angle Resolved Scattering), which are defined in the ASTM standard E2387-05 [1]. This ASTM standard is currently the only active standard available, however, there is a corresponding new ISO standard under development (ISO/WD 19986:2016) [2]. Practically, a quantification of BSDF / ARS is typically performed by in-house developed scatterometers that consequently differ in terms of measurement parameters, optical set-up, and also procedures. This can result in large deviations that are sometimes observed between measurements performed by different laboratories on the same sample. Consequently, a test of the reliability of BSDF measurements and procedures is important for ESA and space optics manufacturers.

Previously performed round-robin experiments of angle resolved light scattering date back to the late 1990s, and were conducted to test the former ASTM E1392 standard [3, 4], which has been by now replaced by ASTM E2387. In addition, round robin experiments have been conducted to verify the standards of the integrated scattering quantities TS (Total scattering, ISO 13696 [4]) and TIS (Total

integrated scattering, ASTM F1048 [5]) [7, 8]. A comprehensive test of the active ASTM E2387 standard for angle resolved scattering has not previously been reported.

This new Round-Robin experiment was part of an ESA-EXPRO project, where ESA, as the project donor, defined the frame conditions, and Fraunhofer IOF, as the project contractor, coordinated the experiments. This paper is organized as follows. Section 2 summarizes the basic light scattering definitions and calibration procedures. Section 3 contains details about how the experiments were organized and conducted, followed by a comprehensive analysis of the results in section 4.

2. Definitions

The BSDF is defined as the surface radiance dL_e scaled by the irradiance dE_e; which equals to the power ΔP_s of the light scattered into the solid angle $\Delta\Omega_s$, normalized to that solid angle, to the incident light power P_i, and to the projected surface area [1,9]

$$\mathrm{BSDF}(\theta_s,\varphi_s)=\frac{dL_e}{dE_e}=\lim_{\Delta\Omega_s\to 0}\frac{\Delta P_s(\theta_s,\varphi_s)}{P_i\Delta\Omega_s\cos\theta_s}, \qquad (1)$$

where φ_s and θ_s are the azimuthal and polar scattering angles (see Fig. 1), respectively. BSDF can be converted into ARS by an additional $\cos\theta_s$ factor, where ARS corresponds to the radiant intensity scaled by the incident radiant flux. It is often convenient to omit the azimuth angle in situations where out of plane scattering can be predicted with adequate accuracy, which is typically the case for moderate angles of incidence and isotropic scattering samples [10].

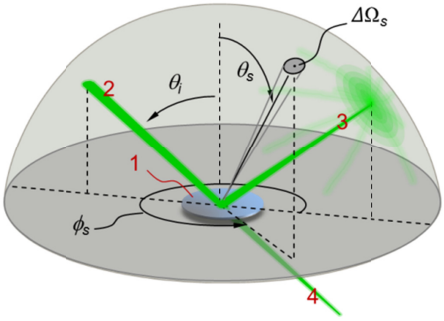

Fig. 1. Light scattering geometry and definitions: 1 - sample, 2 - incident beam, 3 - reflected beam, 4 - transmitted beam, θ_i - angle of incidence, θ_s - polar scattering angle, φ_s - azimuth scattering angle.

Numerical integration of angle resolved quantities allows calculation of the hemispherical scattering quantities or light scattering losses. For normal incidence, integration within θ_s=2° and θ_s=85° corresponds to Total Scattering in the reflection (TS_b) and transmission (TS_f) hemispheres, respectively, as defined in ISO13696 [5]. Integration over the complete hemisphere is sometimes denoted by directional–hemispherical reflectance or total hemispherical reflectance (THR). For different integration limits, the parameter integrated scattering (S) can be used

$$S=\frac{\Delta P_s}{P_i}=\iint BSDF\,\cos\theta_s\sin\theta_s d\theta_s d\varphi \ , \qquad (2)$$

which is denoted by S_f for forward scattering and by S_b for backward scattering, respectively. For the practical measurement of BSDF, a careful instrument calibration is mandatory. Different calibration techniques are suggested in ASTM-E2387, but they all have in common that signal voltage values from the detector are evaluated, rather than measuring the absolute power values P_s and P_i directly, as e.g. comprised in equation (1) and (2). The BSDF can then be calculated by

$$\mathrm{BSDF}(\theta_s,\varphi_s)\approx\frac{V_s(\theta_s,\varphi_s)}{V_i\Delta\Omega_s k_A\cos\theta_s}=\frac{V_s(\theta_s,\varphi_s)}{k_c k_A\cos\theta_s}, \qquad (3)$$

where k_c is a calibration factor that corresponds to $V_i\Delta\Omega_s$. The signal V_s is recorded from the detector during measurement, and V_i corresponds to the detector signal in the incident beam. Hence, in order to measure both extremely low scattering signals from optical components as well as extremely high powers from specular beams, the detection system needs to be working linearly inside a large dynamic range of typically over 10 orders of magnitude. This is usually achieved by adaption techniques that are described by an additional factor k_A. This factor needs to be determined before calibration. Then, different calibration routines can be implemented to determine the other unknown variables:

- Absolute calibration: measurement of V_i while $\Delta\Omega_s$ is calculated from set-up geometries.
- Relative calibration: k_c is determined by measurement of V_s from a reference sample with known BSDF. Recording V_s at multiple scattering angles allows reducing calibration uncertainty. For UV-VIS-NIR measurements, typically white PTFE (Polytetrafluoroethylene) samples are used for calibration.
- Diffuse calibration: k_c is determined by measurement of V_s from a reference sample with known integrated scattering, e.g. TS, where V_s is recorded over the corresponding range of scattering angles and numerically integrated (see also [1]). Typically, white PTFE samples are also used for this calibration.

3. Round-Robin Experiments

A. Layout and organization of the experiments

The large number of participating laboratories required a parallel layout of the experiments to shorten the timescale and to reduce sample contamination during the experiments. In particular, sample contamination, as observed during earlier sequential RR measurement campaigns [7], had to be avoided. One unique sample was measured sequentially by the participants, a quasi-volume-diffuser, that was potentially insensitive to contamination.

In order to find common measurement parameters for the experiments, the participants were asked to provide possible parameters that are feasible with their set-ups and available for the experiments. The most critical measurement parameters were illumination wavelengths, illumination polarization, and the smallest incident angle without obscuration of the reflected beam. This resulted in the following basic measurement parameters:

- Illumination wavelengths (nm): 325, 633, 1064, 1550
- Illumination polarization: s-pol
- Illumination detection: unpolarized
- Incident angle: 11°, except for the grating samples that were measured in Littrow configuration
- Range of scattering angles: -90° to +270° for transparent and diffusor sample (#W and #D samples in section C), opaque samples -90° to +90°
- Scattering angle step sizes: 0.1° for grating samples, other samples 0.5°

A document containing the detailed measurement parameters for the experiments was prepared and sent to the participants. The document also contained sample handling information as well as technical and project management information. ASTM E2387 was the main guide to be followed, although the participants were also free to test their own methods and procedures. After receipt of the samples, the participants were asked to check if the samples had arrived in a good condition. Also, it was advised to use mechanical blowers to blow

off single particles before measurement. Other cleaning techniques were to be discussed with IOF. The participants were requested to find a representative measurement position, therefore it was suggested to laterally scan the surface with fixed incident and scattering angle (usually called raster scan or mapping) prior to the actual BRDF measurement. This allows the identification of local variations of the scattering properties across the sample surface that are often much larger than the actual measurement uncertainty of the instrument [11]. The participants were asked to fill in their results in previously prepared tabular sheets with BSDF and measurement uncertainty ranges (for k=2) as a function of the scattering angle.

The experiments were conducted anonymously. Therefore, each participant received a random number between I and VII, which is correlated with the experimental results instead of with the participant name. The samples were distributed to the participants in June 2015, before that, all samples were screened at the coordinating laboratory. One laboratory joined the experiments in December 2015. The last results and samples were returned to the coordinating laboratory in April 2016. After that, the screening experiments were repeated in order to characterize sample comparability and sample degradation during the experiments (see Fig. 2). These results were eventually correlated with the BSDF data from the participants. An internal report containing results and analysis of the experiments was sent to ESA in July 2016. The internal report for the participants was released in November 2016, and the results were finally presented in June 2017 at ESA-ESTEC.

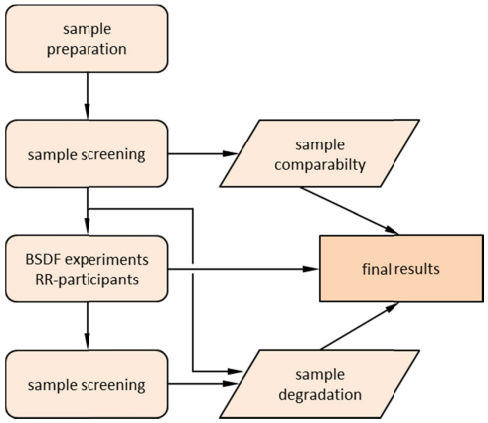

Fig. 2. Schematic of the layout of the experiments.

B. Participating laboratories and instrumentation

Table 1: Laboratories that participated in the RR measurements (alphabetic order)

Designation	Organization
ESA	European Space Agency ESTEC, Noordwijk, The Netherlands
IF	Institute Fresnel, Espace Photonique, Marseille, France
IOF	Fraunhofer Institute for Applied Optics and Precision Engineering, Jena, Germany
LT	Light Tec SARL, Hyères, France
NPL	National Physical Laboratory, Teddington, Middlesex, United Kingdom
TNO	TNO Industrie en techniek, Delft, The Netherlands
TSW	The Scatter Works, Inc., Tucson, Arizona, USA

Seven international laboratories participated in the RR measurements (see Table 1). Complete names, addresses, and other information are listed in Appendix A. Most of the facilities were European research institutions, but also one company from France and one from the USA provided results.

Figure 3 displays the schematics of the different optical set-ups used by the participants. They all incorporate the same fundamental components to measure scattered light, but still have different functional principles and therefore different advantages and disadvantages. The beam from a light source (L) is cleaned by a spatial filter (SF) and illuminates the sample (S). The detection system records the scattered light from the sample with a detector (D), where two apertures are used to define the solid angle (AS) and the field of view (FS). Usually, either a photomultiplier tube or a photo diode is used for measurements in the VIS and NIR. The pinhole is usually imaged onto (AS). Additional detector optics contribute additional scattered light that may affect the near angular limit, nevertheless, they are conveniently used to modify the solid angle or to precisely define the detector field of view.

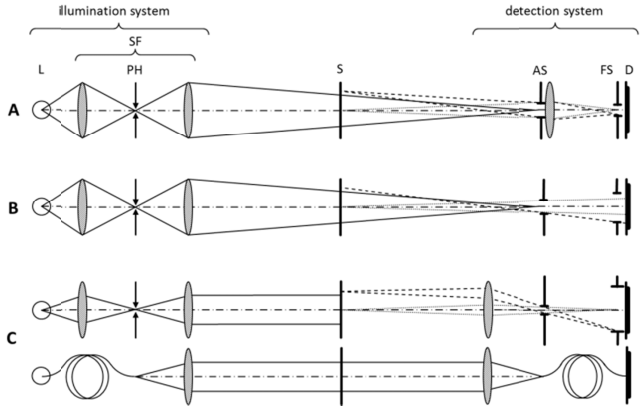

Fig. 3. (Color online) Schematics of the optical designs for angle resolved light scattering instrumentation used by the participants.

The set-ups used by the participants mostly correspond to the optical designs described in the ASTM2387 standard [1]: Set-up (A) corresponds to ASTM design (1), set-up (B) corresponds to ASTM design (2) with exchanged (AS) and (FS) apertures, while set-up (C) corresponds to ASTM set-up (3). One participant used set-up (A) with a modified illumination, such that (PH) is imaged onto (S) and the illumination spot diameter is adjusted by adapting the (PH) size in (SF). One participant extended set-up (C) with fiber optics: the (PH) including the source optics were replaced by a fiber coupled source. On the detection side, this participant also used a collimated detection (symmetric to the illumination) with the aperture (AS) including the detection optics being replaced by a fiber coupled sensor.

Table 2: Set-up and calibration overview of the participants (random order). Participant VII used 2 different set-ups.

Participant number	Set-up	Calibration method
I	A	absolute
II	A	absolute
III	C	absolute
IV	C	relative
V	A	absolute
VI	B	relative
VII	C / C	diffuse / relative

One participant used set-up C where the lens between sample and detector is removed for scattering angles close to the specular beam. One participant used set-up (A) with the over-illumination concept (i.e. the detection field of view is smaller than the illumination spot on the sample). Over-illumination is primarily used to characterize rather highly diffuse scattering samples [12] and typically excels in a highly uniform illumination.

Table 3: Samples for the experiments.

Sample	Substrate / sample type	Front surface	Dimensions (mm)	rms (nm)	Order Number
#M	N-BK7	Al / SiO_2 [85 nm]	ø50.8x9.5	4.3	PAV-PM-2037-C (CVI)
#W	Fused Silica	-	ø50.8x6.35	0.61 / 0.52	PW1-2025-UV (CVI)
#G	Borofloat	reflective holographic grating	25x25x6	40	GH25-12V (Thorlabs)
#S	White PTFE	-	ø40	-	SG 3043-U (Sphere Optics)
#D	Fused Silica volume diffusor	-	ø50x5	500 / 310	HOD-300 (Heraeus)
QVD	2-plate quasi volume diffusor	-	ø60x20	1200	-

For the characterization of low-scattering specular-reflecting samples, it is of most importance to maximize sensitivity, the performance at scattering angles close to the specular beam, as well as to reduce stray light problems. Therefore, the corresponding set-ups use under-filled illumination, small illumination spots (typically about 3 mm of diameter), and are based on laser sources. For the characterization of diffusely-scattering samples, however, high precision is more important than sensitivity or near specular performance. Therefore, a reduction of sample related statistical noise (speckle) is usually achieved by using large illumination spot sizes and/or illumination with an extended spectral bandwidth compared to laser sources.

Two participants used high precision set-ups with effective illumination spot diameters from 5 mm to 8 mm. Broad-band sources also give more freedom in the choice of the illumination wavelength, and were used by three participants. The set-ups and the calibration methods (see also Section 2) used by the participants are summarized in Table 2.

C. Sample set

In order to cover a broad scenario of different experimental challenges for the measurement of scattered light, a possibly comprehensive sample set was to be created. Moreover, all samples from one sample type should be as identical as possible. For this purpose, different suppliers were asked to provide quotes of samples manufactured in one production run. One main condition posed by the project initiator was that the samples had to be available from standard optical suppliers. This posed a challenge for some of the low scattering samples, as the standard quality with respect to sample contamination was not always sufficient for comparable light scattering measurements. Hence, some samples provided had to be rejected. However, all samples were cleaned before shipment using dust-blowers and, if necessary, using drag wiping or ultra-sonic cleaning techniques. All samples were labeled and the front side as well as the azimuthal sample orientation were marked with an arrow.

The final sample set composition is displayed in Table 3. The comprehensive set comprises (i) low and high scattering samples, (ii) specular or diffuse scattering samples as well as diffraction gratings, and (iii) transparent and opaque samples. Of each sample type, one piece for each participants plus one additional spare sample were acquired; except in the case of the QVD sample, where only a single unique piece was used for the experiments.

For typical optical components, light scattering is usually proportional to the interface roughness properties rms roughness and power spectral density function (PSD), for interference coatings the connection is still given but more complex [13-16]. The light scattering relevant rms surface roughness values at λ=633 nm are listed in Table 3 and were derived by topography analysis using atomic force microscopy (AFM) and white light interferometry (WLI) [17-19]. Therefore, master PSD functions were calculated and integrated between 0.055 µm^{-1} and 1.6 µm^{-1} (see Fig. 4). It can be seen that a large range of surface rms roughness values between 0.5 nm and 1.2 µm are covered. One side of the diffusor samples was found to be a rougher than the other side and to exhibit a directional roughness component. This side was defined as the front side. The sample azimuth was orientated such that the direction of highest roughness was orientated in the out-of-plane direction.

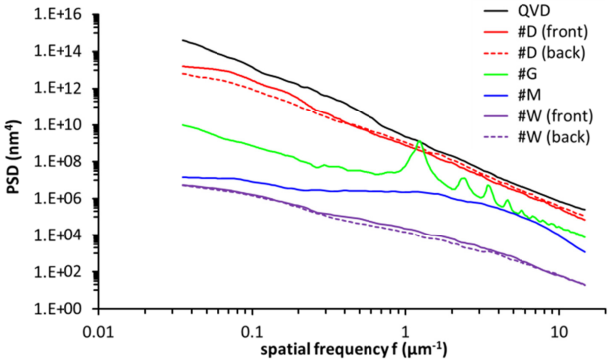

Fig. 4. Master PSD functions of the individual sample types.

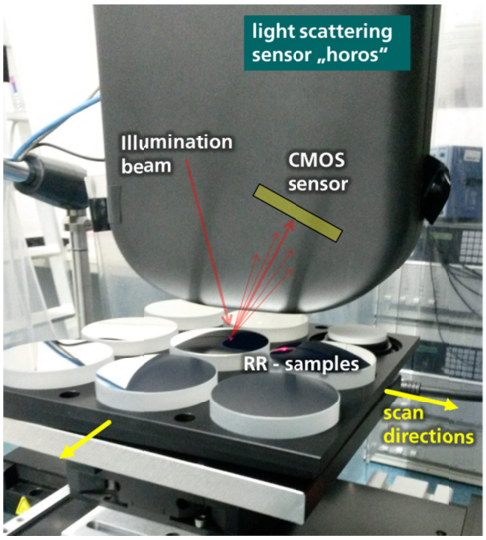

Fig. 5. The samples from each type were screened before the RR experiments in one run using the light scattering sensor "horos". The screening experiments were repeated after the RR experiments. This allowed characterizing the sample comparability as well as sample degradation during the course of the experiments.

D. Sample screening

The samples from each type, respectively, were scanned together in one run using the light scattering sensor "horos" (Fig. 5). This sensor records the near angular scattered light within a cone of 8° around the specular reflection, at an incident angle of θ_i=8°, and at λ=650 nm [20, 21]. It was mounted fixed over an XY-translation sample stage to provide spatially resolved scans of the integrated scattered light S_b of each sample type (integrated between about 1° to 8° around the specular beam). All samples were measured in the reflection hemisphere except for the diffusor samples, which were measured in the transmission direction. The screening experiments were repeated after the RR experiments to analyze sample wear.

As an example, Fig. 6 shows the screening scan for the #M samples before and after the experiments. The second sample in the first row showed the highest deviation from the average and was selected as the spare sample "s" that was not used for the RR experiments. Comparing prescreening and postscreening scans qualitatively already reveals particle contaminations between the scans for participant I, II, and VII.

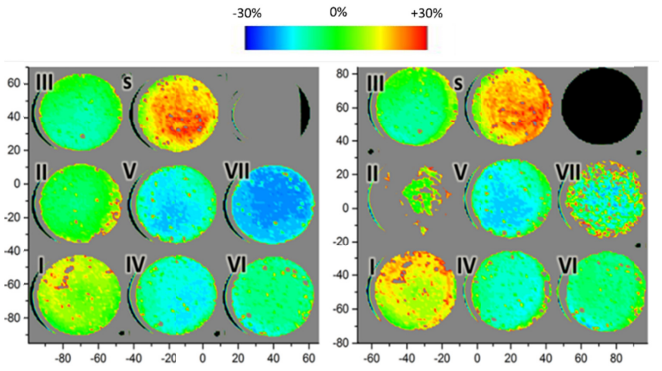

Fig. 6: Comparison of the pre-screening (left) and post-screening (right) results of the eight M# samples. The samples with the highest deviation from the average were removed from the participants' sample pool and marked as spare "s".

Although even this qualitative evaluation would be helpful, a more quantitative post-measurement analysis of these scans is preferable. To derive a single representative integrated scattering value for each sample S_b, the data reduction algorithm suggested in DIN-ISO13696 [5] was applied. The sample comparability $\mathcal{C}$ of sample N is calculated by the relative deviation of its integrated scattering value from the average of the integrated scattering values of all samples $\bar{S}_{b,pre}$:

$$\mathcal{C}_N = \frac{S_{b,pre,N}}{\bar{S}_{b,pre}} - 1 \qquad (3)$$

Based on the scans, spare samples were picked such that comparability and homogeneity of the residual samples were as good as possible. The spare samples were also used to characterize the natural sample wear without human interaction. For this purpose, the spare samples were boxed and stored in a conditioned ISO7 clean room during the RR experiments.

Table 4: Sample comparability $\mathcal{C}_N$ as determined by the pre-screening experiments. The standard deviation (std.) was calculated without the spare samples (s).

	I	II	III	IV	V	VI	VII	s	std.
#M	18%	8%	0%	-5%	-9%	0%	-13%	27%	10%
#W	3%	2%	5%	-21%	8%	1%	2%	-19%	9%
#G	6%	8%	-15%	14%	-14%	8%	-7%	28%	12%
#S	1%	1%	1%	-1%	0%	0%	0%	-1%	1%
#D	-6%	5%	-1%	-1%	0%	5%	-2%	15%	4%

Sample degradation $\mathcal{D}$ of sample N is quantified by the relative change of its integrated scattering value before $S_{b,pre,N}$ and after the experiments $S_{b,post,N}$:

$$\mathcal{D}_N = \frac{S_{b,post,N}}{S_{b,pre,N}} - 1 \qquad (4)$$

For the screening measurements, calibration uncertainties to determine the calibration factor k_c in Equation (3) would result in a constant offset between the pre- and post-screening scans. This was compensated by adapting k_c of the post-screening experiments.

In Table 4 and 5, the results for $\mathcal{C}$ and $\mathcal{D}$ are summarized, respectively. Negative values of sample degradation are a result of measurement uncertainty.

Table 5: Sample degradation $\mathcal{D}_N$ as determined by the pre- and post-screening experiments. The average degradation (avg.) was calculated without the spare samples (s).

	I	II	III	IV	V	VI	VII	s	avg.
#M	4%	264%	1%	3%	0%	1%	14%	1%	41%
#W	0%	215%	-2%	1%	-2%	-1%	98%	2%	44%
#G	3%	9%	2%	1%	-2%	6%	2%	3%	3%
#S	-1%	-1%	-1%	1%	1%	1%	1%	1%	0%
#D	1%	0%	1%	1%	1%	1%	0%	0%	1%

In summary, light scattering related differences between samples (for scattering angles of 1° to 8°) of 1% < $\mathcal{C}$ < 12% have been achieved. Moreover, it can be observed that all spare samples did not exhibit a noteworthy degradation during the experiments. This indicates that effects of natural sample degradation during the course of the RR experiments can probably be excluded. Highest degradation caused by sample handling during the experiments was observed for the low scattering samples #M and #W, while the high scattering samples did not show a significant degradation.

4. Results

A total of 73 BSDF measurements were provided by the 7 participants (see Annex B). Additional data processing was necessary to evaluate the results, as some participants provided data in other coordinate systems, with a different sampling of the scattering angle, in ARS instead of BSDF, or with unremoved measurement artifacts.

A. Comparison by integrated scattering values

To effectively compare this huge number of measurements, a single parameter per angle resolved scan is beneficial. For this purpose, the angle resolved scans were numerically integrated in regions of θ_s where no measurement artifacts (especially detector obscurations and influences from the instrument signature) were expected and where all participants delivered data. Before integration, the BSDF measurements were shifted to normal incidence according to the shift invariance postulated by Harvey [22], except for the QVD and #S samples. Then, the data were interpolated on a 0.1° grid on a vertical log scale and integrated to yield S_b by means of Equation (2). Integration ranges from +5° to +50° in reflection direction and +125° to +175° in transmission direction were used, except for the QVD sample (integration limits between +185° to +235°), the #D samples (integration limits between +140° to +175° and +5° to +35°, respectively), and the #G samples (integration limits between 0° to +5°). The calculated integrated scattering values are plotted in Figures 7 to 12 for all provided measurements of the individual sample types.

From these values and per illumination wavelength, the standard deviation of the integrated scattering values was calculated, and their relative deviations from the arithmetic mean were calculated. The

standard deviation was also calculated even if the number of provided measurements was in part too low for statistically significant results. In tables 6 to 11, these deviations are directly compared to sample comparability and sample degradation. Outliers (identified by wavelength scaling or experience based on observed deviations between the reported data and the expected shape of the BRDF for each specific type of measurement artefact) were removed and not included in the calculations.

1. Mirror samples #M

Figure 7 and Table 6 show the results of the #M samples. Integrated scattering decreases with increasing illumination wavelength, as would be expected for smooth samples that scatter purely from the topography. Two outliers were observed by comparison and by wavelength-scaling analysis (see Appendix C). These outliers were probably caused by calibration issues; however, for the measurement at 1550 nm sample degradation effects are also possible. The prescreening results revealed that participant I received an 18% higher scattering sample than the sample average (see Table 6). This effect could possibly be present in the 325 nm measurements, but cannot be observed for 633 nm illumination. Besides the outliers, the measurements show a very good overall agreement with a standard deviation of 9% for all illumination wavelengths.

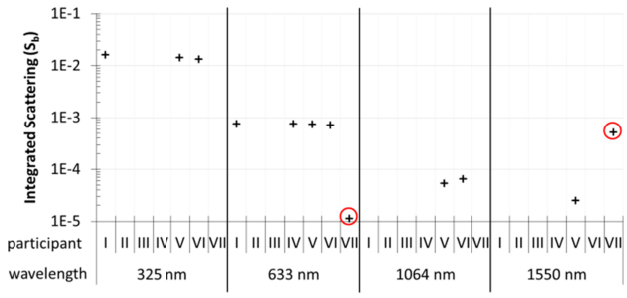

Fig. 7: Comparison of the #M sample measurements. Outliers marked by red circles.

Table 6: Analysis of the measurement deviations of the #M samples with outliers removed.

	I	II	III	IV	V	VI	VII	std.
$\mathcal{C}$	18%			-5%	-9%	0%	-13%	12%
$\mathcal{D}$	4%			3%	0%	1%	14%	-
325 nm	11%				-3%	-9%		10%
633 nm	2%			2%	0%	-4%	OL	3%
1064 nm					-10%	10%		14%
1550 nm					0%		OL	-

2. Window samples #W

Figure 8 and Table 7 show the results of the #W samples. Integrated scattering decreases with increasing illumination wavelength. Outliers were observed by comparison and by observation of the wavelength-scaling characteristic. The shape of the BSDF measurements from participants VII at 633 nm and 1550 nm could indicate sample degradation effects (see Fig. 22 in Annex B). The 1550 nm measurement of participant V is probably affected by noise effects (the data also contained negative BSDF values). A similar deviation of the prescreening result compared to the 633 nm BSDF measurement of participant IV indicates a possible sample comparability related effect. Besides the outliers, the measurements exhibit an average standard deviation of 40%, which is considered reasonable within the constraints and expectations of this comparison, as light scattering measurement on transparent low scattering optics are more easily affected by straylight or contamination issues.

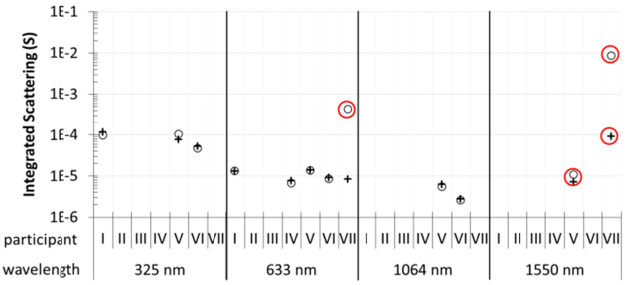

Fig. 8: Comparison of the #W sample measurements. Outliers marked by red circles; forward scattering S_f / backward scattering S_b indicated by circles / crosses, respectively.

Table 7: Analysis of the measurement deviations of the #W samples with outliers removed.

		I	II	III	IV	V	VI	VII	std.
$\mathcal{C}$		3%			-21%	8%	1%	2%	11%
$\mathcal{D}$		0%			1%	-2%	-1%	98%	-
S_b	325 nm	42%				-7%	-36%		39%
	633 nm	25%			-27%	34%	-12%	-20%	28%
	1064 nm					38%	-38%		54%
	1550 nm					OL		OL	-
S_f	325 nm	18%				26%	-43%		38%
	633 nm	27%			-37%	29%	-19%	OL	33%
	1064 nm					36%	-36%		50%
	1550 nm					OL		OL	-

3. Grating samples #G

Figure 9 and Table 8 show the results of the #G samples, again, the integrated scattering values decrease with increasing illumination wavelength. No outliers were observed. The low BSDF values at scattering angles between -90 and -70° in the 325 nm measurement of participant I (see Fig. 23) could be caused by sample holder obscuration, also, a slightly misaligned incident angle was observed for this measurement, which specifically affected the angular position of the specular reflected and diffracted peaks. Sample comparability effects could have affected the 633 nm measurements of participant IV, and the 1064 nm measurements of participant V and VI. An average standard deviation of 22% was found for this sample type. However, it should be noted that at large scattering angles the deviations are even significantly higher than this (see section 4.2, Fig. 15), which serves to emphasis the extreme difficulty associated with making BRDF measurements on gratings.

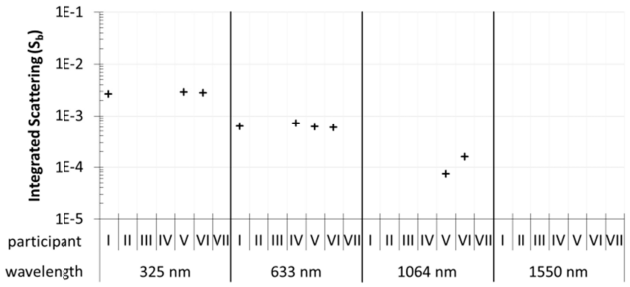

Fig. 9: Comparison of the #G sample measurements. No outliers were observed.

Table 8: Analysis of the measurement deviations of the #G samples. No outliers were observed. No data was provided for 1550 nm.

	I	II	III	IV	V	VI	VII	std.
$\mathcal{C}$	6%			14%	-14%	8%		12%
$\mathcal{D}$	3%			1%	-2%	6%		-
325 nm	-6%				5%	1%		5%
633 nm	-1%			12%	-4%	-6%		8%
1064 nm					-36%	36%		52%
1550 nm								-

4. PTFE samples #S

Figure 10 and Table 9 show the results of the #S samples. The derived sample comparability was below the measurement uncertainty of the prescreening set-up. These samples are especially interesting as white PTFE is often used for the calibration of optical systems - including instruments for the measurement of scattered light when the calibration methods "relative" or "diffuse" are used. These samples typically exhibit a rather constant TS in the specified spectral bandwidth, which is between about 250 nm and 2500 nm. Hence, the integrated scattering values show no significant trend as a function of the illumination wavelength. Two outliers were observed for participant V, indicating a calibration issue. Also, some of the contributed BSDFs are slightly asymmetric indicating sample/system misalignment issues.

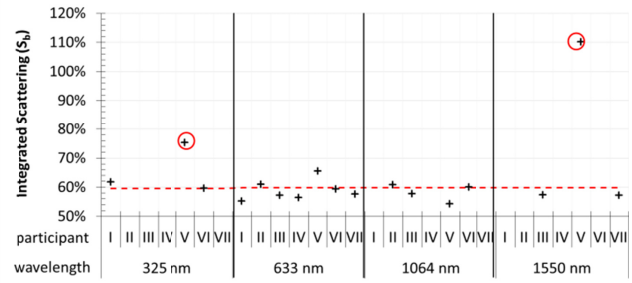

Fig. 10: Comparison of the #S sample measurements. Outliers marked by red circles.

The measurements were additionally compared to the vendor specification of a sample from the same sample type. The vendor's measurements are for unpolarized illumination (instead of s polarized light) with 8° incident angle (instead of 11° incident angle) and hemispherical collection (instead of integration between scattering angles of +5° and +50°) . Hence, in order to make a comparison with the RR results, a representative BSDF for the sample was first obtained, based on the mean of the BSDF curves for the participants at 633 nm with outliers removed, This average BSDF curve was then corrected by a factor to yield the hemispherically scattered light value, which was given by the vendor for the individual wavelengths. Then, the corrected curves were integrated over the same scattering angles as the RR measurements, which could then be directly compared with the S_b value of each participant. We want to note that these calculated values derived from the vendor specification do not represent the "correct" results but can be seen as an additional source of comparison.

Besides the outliers, the measurements show a good overall agreement with an average standard deviation of 3%.

Table 9: Analysis of the measurement deviations of the #S samples with outliers removed. The data were also compared to the vendor specification VS.

		I	II	III	IV	V	VI	VII	std.
	$\mathcal{C}$	1%	1%	1%	-1%	0%	0%	0%	1%
	$\mathcal{D}$	-1%	-1%	-1%	1%	1%	1%	1%	0%
	325 nm	2%				OL	-2%		2%
	633 nm	-6%	3%	-3%	-4%	11%	1%	-2%	6%
	1064 nm		5%	-1%		-7%	3%		5%
	1550 nm			0.2%		OL		-0.2%	0.3%
VS.	325 nm	4%				OL	0.1%		3%
VS.	633 nm	-8%	1.9%	-4%	-6%	10%	-1%	-4%	6%
VS.	1064 nm		1.6%	-4%		-9%	0.4%		5%
VS.	1550 nm			-4%		OL		-4%	0.3%

5. Diffusor samples #D

The results of the volume diffusor samples are summarized in Fig. 11 and Table 10. Only marginal wavelength scaling properties can be observed. The measurements showed a surprisingly large amount of outliers, identified by a (typically too low) scattering value or a distinctive asymmetric characteristic of the BRDF curves (see Annex B Fig. 26). These are probably caused by detector field of view and system/sample misalignment issues: As a result of volume scattering effects, small illumination spots spread to a large area on the surface of the diffusor. This is in conflict with the detector field of view (FOV) which is usually minimized for under-illumination instruments - if the FOV is smaller than the light scattering area, the measured BSDF is artificially too low. If the outliers are excluded, the average standard deviation of the measurements is 4%.

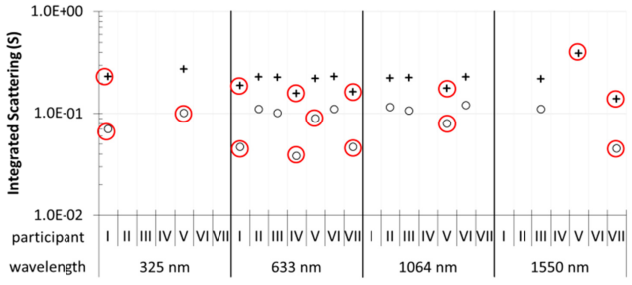

Fig. 11: Comparison of the #D sample measurements. Outliers marked by red circles; forward scattering S_f / backward scattering S_b indicated by circles / crosses, respectively.

Table 10: Analysis of the measurement deviations of the #D samples with outliers removed.

		I	II	III	IV	V	VI	VII	std.
	$\mathcal{C}$	-6%	5%	-1%	-1%	0%	5%	-2%	4%
	$\mathcal{D}$	1%	0%	1%	1%	1%	1%	0%	1%
S_b	325 nm	OL				0%			-
S_b	633 nm	OL	0.8%	-0.2%	OL	-2%	2%	OL	2%
S_b	1064 nm		-1.0%	-0.2%		OL	1%		1%
S_b	1550 nm			0%		OL		OL	-
S_f	325 nm	OL				OL			-
S_f	633 nm	OL	3%	-5%	OL	OL	3%	OL	5%
S_f	1064 nm		1.2%	-7%		OL	6%		6%
S_f	1550 nm			0%				OL	-

6. QVD sample

The results for the QVD sample are displayed in Fig. 12 and in Table 11. This unique sample was measured by the participants sequentially in the order I, VI, II, V, IV, III, VII. Similarly to the diffusor samples, the

BSDF measurements show relatively large deviations in shape of the distribution, with outliers again being identified by low scattering values, probably caused by FOV and system/sample misalignment issues.

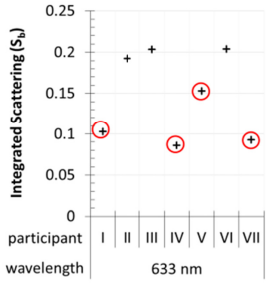

Fig. 12: Comparison of the QVD sample measurements. Outliers marked by red circles.

Table 11: Analysis of the measurement deviations of the QVD samples with outliers removed.

	I	II	III	IV	V	VI	VII	std.
633 nm	OL	-4%	2%	OL	OL	2%	OL	3%

B. Measurement uncertainties and deviations

The BSDF measurement uncertainty is sometimes roughly estimated as near 10% for high dynamic range measurements [11]. However, it is sometimes reported to be substantially lower than this for the characterization of diffuse scattering samples with a comparatively high and constant scatter level, e.g. Spectralon®, where uncertainties of about 0.2% have been reported [23-25].

The GUM (Guide to the expression of uncertainty in measurement) [26] has been developed to provide an international consensus for the expression of uncertainty in measurements. However, a detailed measurement uncertainty evaluation of angle resolved light scattering instruments is particularly difficult. This is because BSDF measurement uncertainty is influenced by a large number of parameters, e.g. signal drifts, detector non-linearity, positioner accuracies, signal noise, reference sample inhomogeneity / anisotropy, calibration uncertainties, signal adaption uncertainty (e.g. from gain level or optical attenuator changes), etc., but also instrument and sample (mis-)alignment. Moreover, sample inhomogeneity and speckle effects can lead to uncertainties significantly larger than scatterometer related uncertainties.

Some participants did not contribute measurement uncertainty budgets for their BSDF measurements. One participant stated a general accuracy of <1%; another participant reported a stability between 0.3% and 2.1% (mainly depending on wavelength). Participants II and III were the only laboratories that contributed results with detailed BSDF measurement uncertainty models as a function of the scattering angle. These participants also used set-ups with a focus on a low measurement uncertainty rather than high sensitivity. They provided their measurements with very low uncertainty ranges between ΔBSDF/BSDF=0.2% and 1%.

Unfortunately, participant III used unpolarized illumination instead of s-polarized illumination because of budget restrictions. This limits the comparability of the results with participant II, and does not allow a concluding evaluation of the measurement uncertainty budgets, however, an angle resolved comparison of the uncertainties is still interesting and therefore discussed (#S and #D samples). For the #M, #W, and #G samples, no participant provided angle resolved uncertainties. Hence, for these sample types, only the relative standard deviation of the BSDF results σ(BSDF) / μ(BSDF) is analyzed, where μ(BSDF) is to the average BSDF(θ_s) that was measured by the participants, and where σ(BSDF) is the corresponding standard deviation of the BSDF(θ_s) functions from all participants (without outliers). For the other sample types additionally the relative deviation $BSDF_{III}/BSDF_{II}$ - 1 between the measurements of participant II ($BSDF_{II}$) and III ($BSDF_{III}$) is directly compared to their measurement uncertainties. Only the measurements at 633 nm are compared, where most participants provided results. Again, outliers were not included into the analysis.

1. Mirror samples #M

The angle resolved relative standard deviation of the #M sample measurements is displayed in Figure 13 (with outliers removed). The deviation is clearly a function of the scattering angle, with deviations between about 3% and 30% for $|\theta_s-\theta|>2°$, while the largest deviations can be observed near the specular beam and for large scattering angles. This clearly exceeds sample comparability (12% for the samples of I, IV, V, and VI) and degradation. Moreover, these deviations are significantly higher than the sometimes stated uncertainties of near 1% or 2%. The higher fluctuations in the BSDF of participant VI are probably related to speckle and/or signal noise.

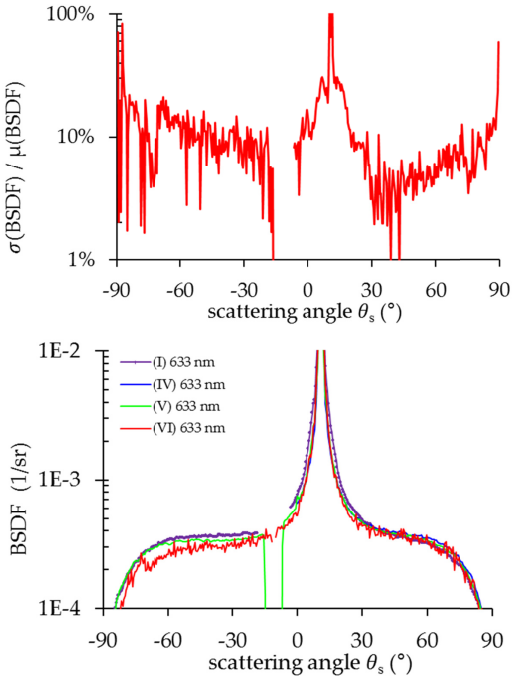

Fig. 13: Relative standard deviations (top) and BSDF results (bottom) of the #M sample measurements at λ=633 nm for all participants that measured this sample (outliers removed).

2. Window samples #W

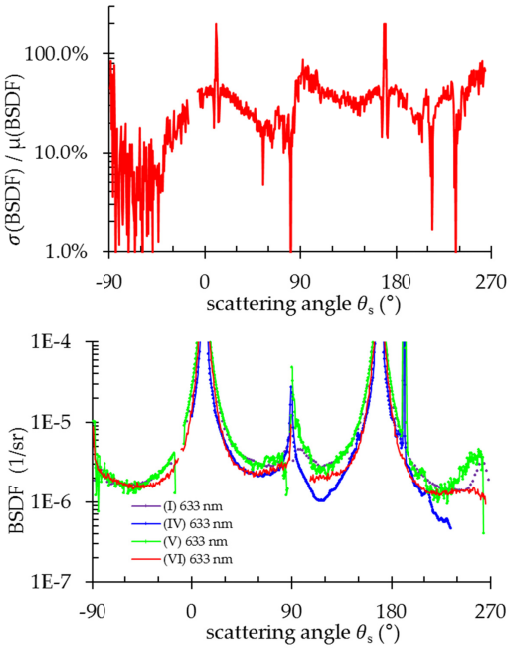

Fig. 14: Relative standard deviations (top) and BSDF results (bottom) of the #W sample measurements at λ=633 nm for all participants that measured this sample.

The angle resolved relative standard deviation of the #W sample measurements is displayed in Figure 14. Again, it is clearly a function of the scattering angle, with deviations between about 6% and 80% for scattering angles larger than 2° away from the specular beams. And again, the largest deviations can be observed near the specular beam and for large scattering angles. This is significantly higher than sample comparability (13% for the samples of I, IV, V, and VI), sample degradation, and reported uncertainties.

3. Grating samples #G

The angle resolved relative standard deviation of the #G sample measurements is displayed in Figure 15. As for the mirror and window samples, it is a function of the scattering angle and varies between about 10% and 100% for scattering angles larger than 2° away from the specular diffracted beams. The largest deviations are once more near the specular beams and at large scattering angles, and exceed sample comparability (12% for the samples of I, IV, V, and VI), sample degradation, and reported uncertainties.

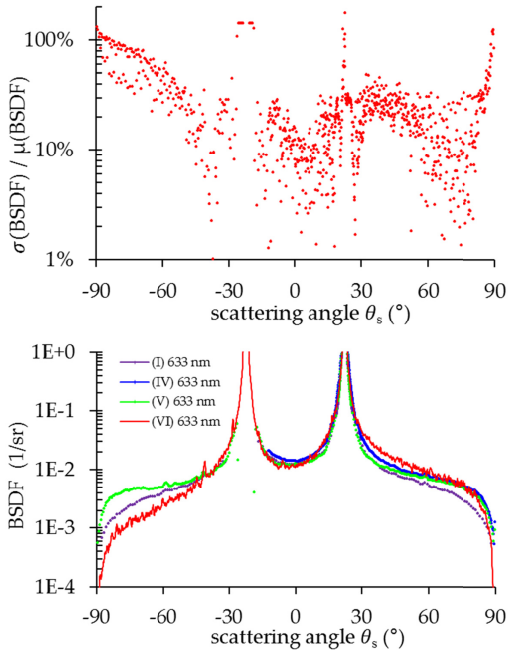

Fig. 15: Relative standard deviations (top) and BSDF results (bottom) of the #G sample measurements at λ=633 nm for all participants that measured this sample.

4. PTFE samples #S

A comparison of the #S measurements at λ=633 nm is shown in Figure 16. The relative standard deviation was found to be almost constant over the scattering angle, at about 8%, while the peak-to-valley deviation of the measurements of participant V and I correspond to about 16%. Compared to the measurements of participant II and III, most measurements exhibit a higher level of noise and larger deviations. Also, asymmetries can be observed, possibly related to sample / instrument alignment effects.

The BSDF measurements of participant II and III differ by about 6% (see Fig. 17), with no overlap in the uncertainty ranges. The differences are unlikely to be due to sample comparability effects, since the screening checks showed these deviations should be below about 1%. Similarly, anisotropy effects larger than 1% would have been noticed in the prescreening experiments and can probably also be excluded. Previous measurements on PTFE samples of a different supplier showed only small azimuthal deviations of about 1% [27, 28]. However, it is important to note that these participants used different polarization conditions (participant II used s-polarized light, while for participant III it was unpolarized). Polarization effects in the range of 1%-2% have previously been observed for PTFE samples, however, from a different supplier [29]. As the PTFE samples used during the experiments have not been characterized for polarization properties, polarization effects cannot be excluded and could possibly account for the 6% difference observed for the measurements of participant II and III. Hence, the role of measurement uncertainties on the deviations is not clear.

It is interesting to note that if the BSDF data are integrated assuming isotropy and normal incidence (in fact an incident angle of 11° was used and the sample could show minor anisotropic behaviour), the calculated THR values are 101% and 95% for participant II and III, respectively. Scaling the curve of participant II to a THR of 98.9% (vendor specification for unpolarized light) yields the dashed line, which is somewhere between the results of both participants.

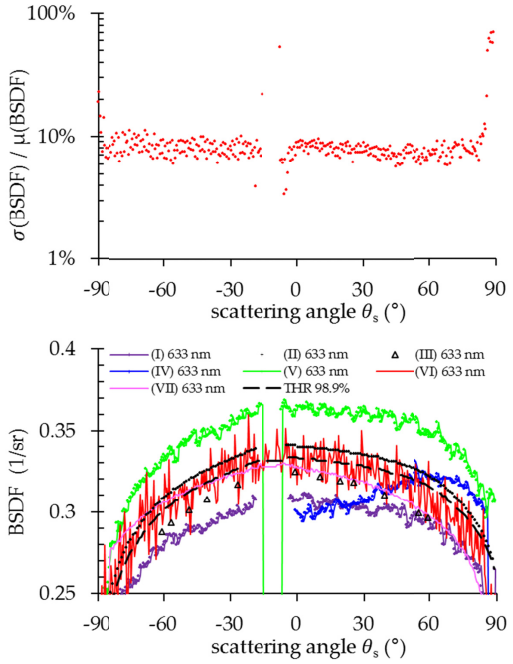

Fig. 16: Relative standard deviations (top) and BSDF results (bottom)of the #S sample measurements at λ=633 nm of all participants.

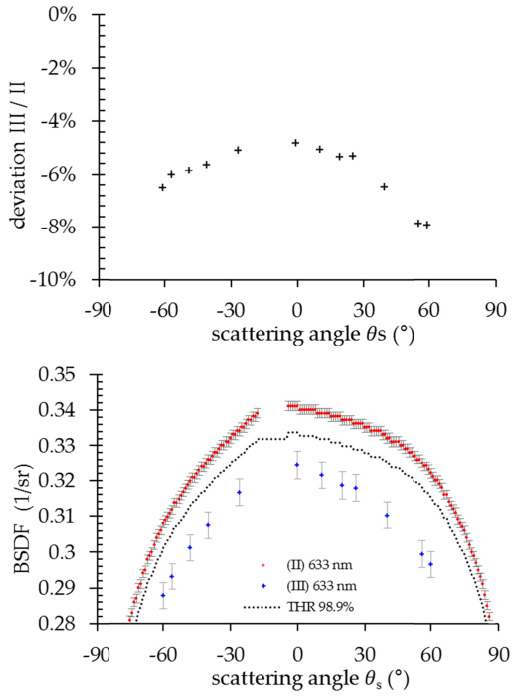

Fig. 17: Comparison of the deviations (top) and the BSDF results and uncertainties of the #S sample measurements at λ=633 nm for participant II and III. The error bars correspond to uncertainties at k=2. The dotted line corresponds to the scaled BSDF of an #S sample with a THR according to the vendor specification.

4. Diffusor samples #D

The angle resolved relative standard deviation of the #D sample measurements is displayed in Fig. 18. Standard deviations between about 2% and 4% can be observed for the majority of the scattering angles, although deviations at very large angles exceed 10%.

For the diffusor samples, the measurements of participant II and III deviated by about +8% for forward scattering, and +1% for backward scattering; the uncertainty ranges do not overlap. The deviations of their results, however, correlate with the sample comparability from the prescreening tests, which was determined in forward scattering direction to deviate by +6% between those two participants. Hence, the deviation of these measurements is presumably caused by sample comparability effects rather than measurement uncertainty.

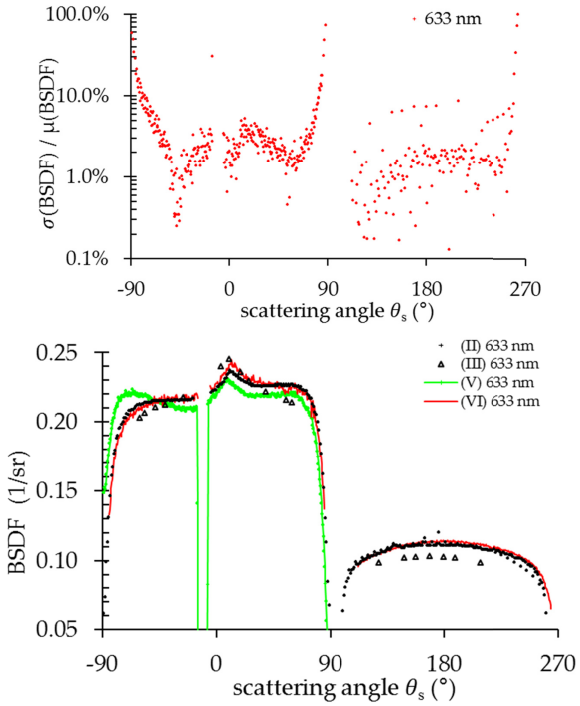

Fig. 18: Relative standard deviations (bottom) and BSDF results (top) of the #D sample measurements at λ=633 nm.

6. QVD sample

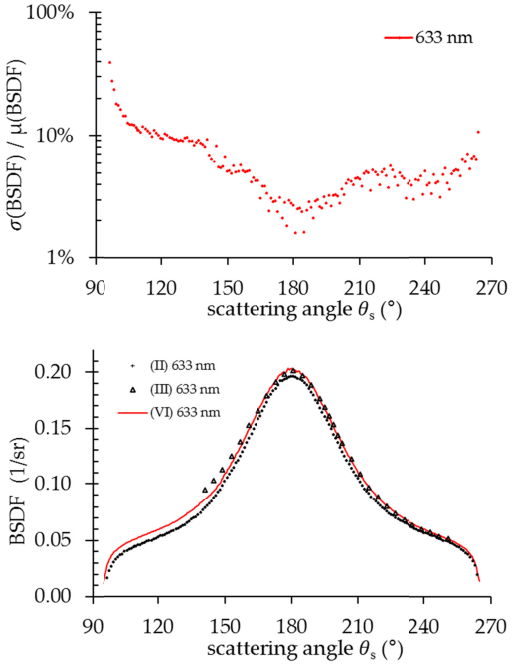

Fig. 19: Relative standard deviations (bottom) and BSDF results (top) of the QVD sample measurements at λ=633 nm of all participants.

The relative standard deviations of the QVD sample measurements (Fig. 19) range between about 2% and 10% for the majority of scattering angles.

The measurements of participant II and III deviate between 2% and 18% (no measurement uncertainty overlap). However as with other samples, it is important to note the different illumination conditions. Moreover, sample inhomogeneity effects may be important, as participant III measured in the center of the sample, while participant II chose a measurement position 20 mm from the sample center. Possible sample non-uniformity influence is supported by the measurement of participant VI, who also performed the measurement in the center of the sample, with good agreement to the measurement of participant III.

C. Additional comments on measurement uncertainty specifications

For the specular samples (#M, #W, #G samples), the observed standard deviations showed the following characteristics: the deviations exhibited both (i) a function of the scattering angle as well as (ii) a function of the sample type. This clearly contradicts the often-used approach of specifying a general single-value measurement uncertainty for light scattering instrumentation. Moreover, the observed deviations significantly exceeded typical claimed general measurement uncertainties of around 1% or 2%.

As effects from sample comparability or degradation are considered unlikely (see screening experiments), a possible explanation for the significant deviations close to the specular beam and at large scattering angles is alignment uncertainty. Fig. 20 shows the measured BRDF and the modeled measurement uncertainty of an aluminum coated substrate [30]. The light scattering distribution exhibits a similar shape compared to that of the #M samples. Also, the shape and level of the resulting total measurement uncertainty are very similar to the angle resolved standard deviation of the #M sample measurements. In the model, different typical scatterometer related contributions were considered, as e.g. signal noise or non-linearity. Moreover, the impact of instrument and sample misalignment on the BSDF measurement uncertainty was determined by simulating typical alignment strategies with the Monte-Carlo method. The simulations showed, that misalignment causes measured BSDF values to be assigned to wrong scattering angles. This effect on the BSDF measurement uncertainty is especially significant, when the slope in the BSDF is high. As a result, the combined uncertainty is not constant over all scattering angles and is dominated by alignment errors at very large angles of θ_s and for scattering angles close to the specular directions where the slope in the BSDF is very high.

Similar effects can also be observed for the diffuse scattering samples, where the relative BSDF standard deviations also showed a function to both the scattering angle as well as the sample type.

Strictly speaking, BSDF measurement uncertainties can actually only be given, if the BSDF is already known, i.e. for already performed measurements. Hence, for the specifications of light scattering instruments, the measurement uncertainty could be given for typical ideal samples, e.g. an ideal Lambertian scattering sample with 100% THR (BSDF=1/π), or e.g. an aluminum mirror with 1 nm rms surface roughness and constant slope in the BSDF (which corresponds to s=-2 and b=0.17 for a 2 parameter Harvey model [22] at λ=633 nm).

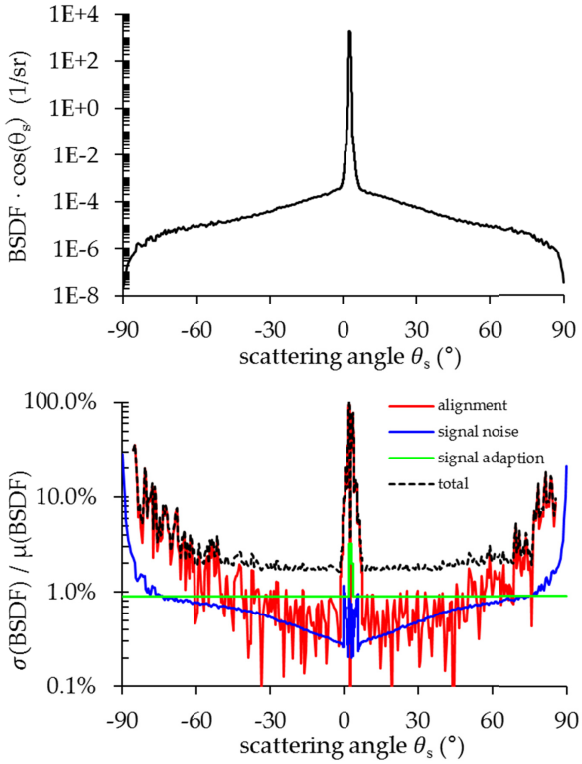

Fig. 20: Measured BRDF (top, λ=532 nm) with calculated measurement uncertainty (bottom, k=2) of an Aluminum coated substrate with different uncertainty contributions.

6. Summary

An international Round-Robin experiment for angle resolved light scattering measurements was successfully conducted. Seven institutions and companies from Europe and the USA participated in the experiments, using different set-ups and procedures. ASTM E2387-05 was used as the main guide, and the experiments were conducted anonymously.

Six different sample types were to be measured, including transparent substrates, Al/SiO_2 coated substrates, grating samples, PTFE calibration standards, volume diffusors, and a quasi-volume diffusor. For the experiments, each participant received their own set of samples (parallel layout of the experiments), while one unique sample was measured by all participants sequentially. To characterize sample comparability and degradation, the samples were screened before and after the experiments. Sample comparabilities between <1% and 12% were observed depending on the sample type. Contamination / sample degradation during the experiments was highest for the low scattering samples (substrates and mirror coated samples), while a contamination related effect on the light scattering distributions of the diffuse scattering samples (PTFE and diffusor samples) could not be observed. This confirms the necessity of parallel experiments for low scattering samples; however, for future RR experiments, a sequential measurement of diffuse scattering samples could be beneficial.

The experiments showed reasonable agreements, mainly depending on the sample type. However, in some cases significant deviations of outliers of up to 2 orders of magnitude were identified, probably caused by calibration issues. When outliers are excluded, standard deviations of the integrated scattering between 3% and 39% were observed for low scattering samples, while the diffuse scattering samples showed deviations between 2% to 6%.

Not all particpants provided measurement uncertainty ranges according to GUM, often, a single general scatterometer-related measurement uncertainty value was stated. Comparing the angle resolved standard deviations of the BSDF measurements (rather than the integrated scattering values), it could be observed that the deviations exhibited, were both a function of the scattering angle as well as of the sample type. This clearly contradicts the often-used approach of specifying a general single-value measurement uncertainty for light scattering instrumentation. With angle resolved standard deviations between about 3% and 100% for the low scattering samples, the deviations were moreover larger than sample comparability and generally-quoted scatterometer measurement uncertainties of about 1% or 2%. Highest deviations occurred at near specular scattering angles and very large scattering angles. This behavior can be explained by alignment uncertainties of instrument and sample [30], which increase for high slopes in the BSDF. Quoting BSDF measurement uncertainties for typical samples rather than giving a single number could solve this problem.

The volume diffusor and quasi volume diffusor characterization unexpectedly turned out to be very challenging. Systematic errors during the measurement of these samples were linked to detector field of view and alignment issues.

The limited budget of this study required a voluntary contribution of the BRDF measurements by all participants and also caused some aspects not to be studied in full detail. Still open subjects are, for example, (i) a study to analyze if the deviation of the BSDF measurements of participant II and III can be related to polarization effects, (ii) a detailed investigation of the critical near angle scattering uncertainty, (iii) experiments on curved optics and black coatings, and (iv) an investigation of the relationship between high sensitivity and high accuracy measurements.

However, in summary, the experience learned is very useful for the participants, the community, and the development of the new ISO standard. For example, a general performance of raster scans before the actual BSDF measurement should be recommended to help deriving sample representative data by avoiding measurements at positions with local defects, e.g. as already addressed in ISO13696. Moreover, a general agreement on data handling should be developed, including e.g. the removal of measurement artifacts from the BSDF data. Also, a general delivery of instrument signature data along with the actual BSDF measurement data would give optical engineers a better insight, as it allows identifying where the measurements are potentially influenced by measurement artifacts or limitations of the used set-up.

Acknowledgment and funding. First we want to thank all the participating institutions and companies for their voluntary contribution and for providing the necessary budget. We also thank Christian Wiede (IOF) for support and sample preparations. We gratefully acknowledge Sandra Müller (IOF) for ultrasonic cleaning. Luisa Coriand and Nadja Felde (both IOF) are thanked for the topography measurements and the PSD analysis.
This study was part of the ESA-EXPRO project "BSDF Round-Robin Measurements of Diffuse, Specular, and Gratings Samples", ESA Contract No. 4000112630/14/NL/PA, according to the Request for Proposal RFP IPL-PTM/PA/gm/510.2014 and the Statement of Work (SoW) Appendix 1 to RFP 510.2014 SoW, 2014.

Annex A: Names and Addresses of the Round-Robin Participants

Sakina Achour, Maryvonne Chalony, Quentin Kuperman, Yan Cornil: Light Tec SARL, Pôle d'Activités Hyérois, 1128 Route de Toulon, 83400 Hyères, France; phone: +33 494 121848; e-mail: sakina.achour@lighttec.fr, maryvonne.chalony@lighttec.fr, quentin.kuperman@lighttec.fr, and yan.cornil@lighttec.fr.

Agnieszka Bialek, Teresa Goodman, Claire Greenwell: National Physical Laboratory, Hampton Rd, Teddington, Middlesex, TW11 0LW, United Kingdom; phone: +44 208 943 6716; e-mail: agnieszka.bialek@npl.co.uk, teresa.goodman@npl.co.uk, c.l.greenwell@soton.ac.uk.

Bilgehan Gur, Sanneke Brinkers, Gerard Otter, Amir Vosteen: TNO Industrie en techniek, Stieltjesweg 1, 2628 CK Delft, The Netherlands; phone: +31 88 866 4657; email: bgur1258@gmail.com, sanneke.brinkers@tno.nl, gerard.otter@tno.nl, amir.vosteen@tno.nl.

Michel Lequime, Myriam Zerrad, Simona Liukaityte, and Claude Amra: Institute Fresnel, Domaine Universitaire de Saint Jérôme, 13397 Marseille cedex 20, France; phone: +33 4 91 28 87 16; email: michel.lequime@fresnel.fr, myriam.zerrad@fresnel.fr, simona.liukaityte@gmail.com, and claude.amra@fresnel.fr

John C. Stover: The Scatter Work, Inc., 2100 N. Wilmot, Suite 202, Tucson AZ 85712, USA; phone: +1 520 325 6323; email: john@thescatterworks.com.

Ramon Vink, Atul Deep, Dominic Doyle: European Space Agency ESTEC, Optics Section (TEC-MMO), Keplerlaan 1, PO Box 299, 2200 AG Noordwijk, The Netherlands; phone: +31 71 565 3634; e-mail: Ramon.Vink@esa.int, atul.deep@esa.int, dominic.doyle@esa.int.

Alexander von Finck, Tobias Herffurth, Angela Duparré, and Sven Schröder: Fraunhofer Institute for Applied Optics and Precision Engineering IOF, A.-Einstein-Str. 7, 07745 Jena, Germany; phone: +49 3641 807-232, e-mail: alexandervonfinck@web.de, Tobias.Herffurth@iof.fraunhofer.de, Angela.Duparre@iof.fraunhofer, and Sven.Schroeder@iof.fraunhofer.de.

Annex B: Results

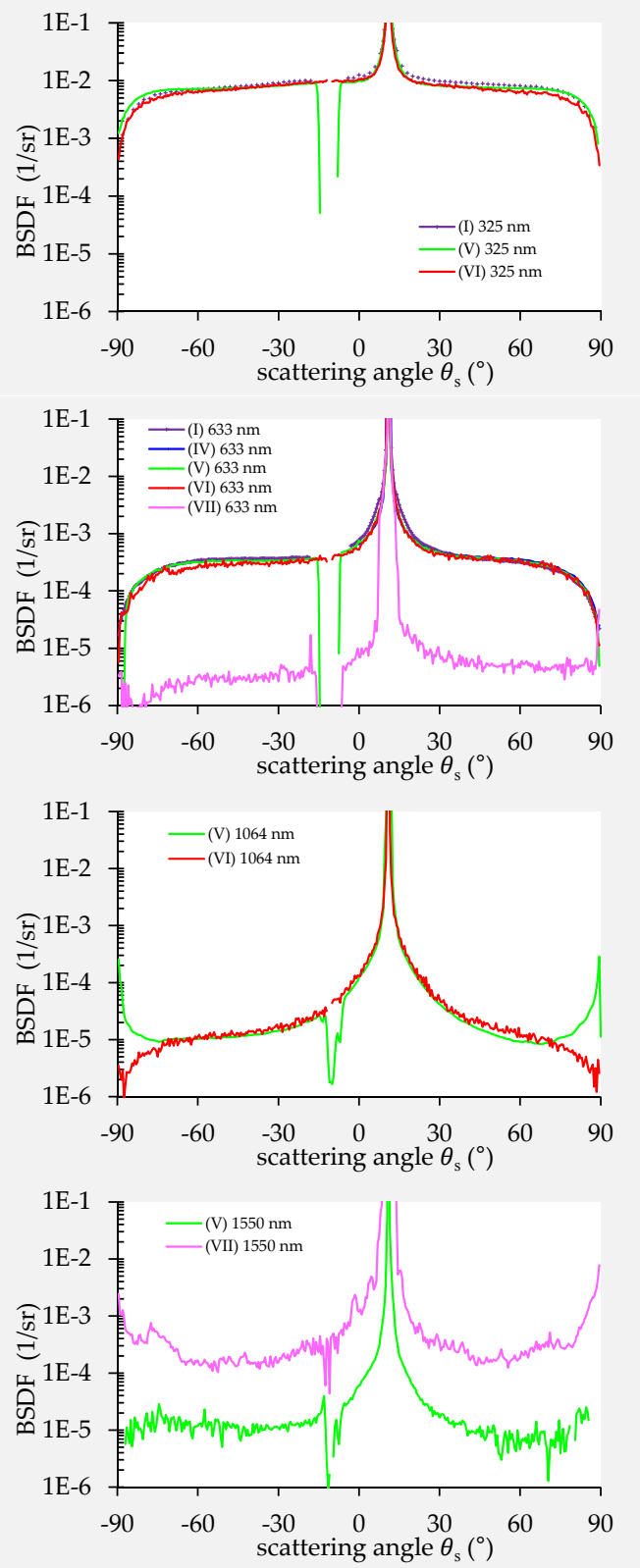

Fig. 21: RR measurements of the M# samples (Aluminum / SiO_2 coated BK7 substrate).

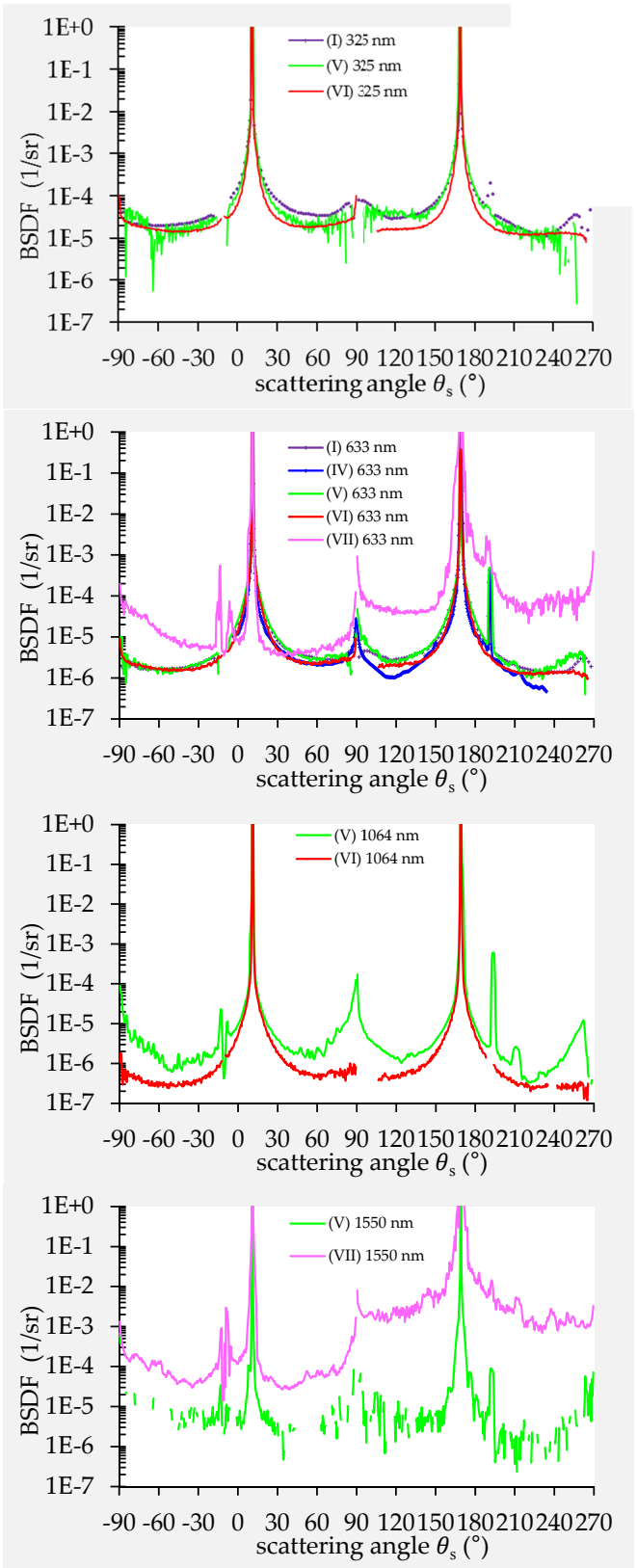

Fig. 22: RR measurements of the W# samples (fused silica substrate).

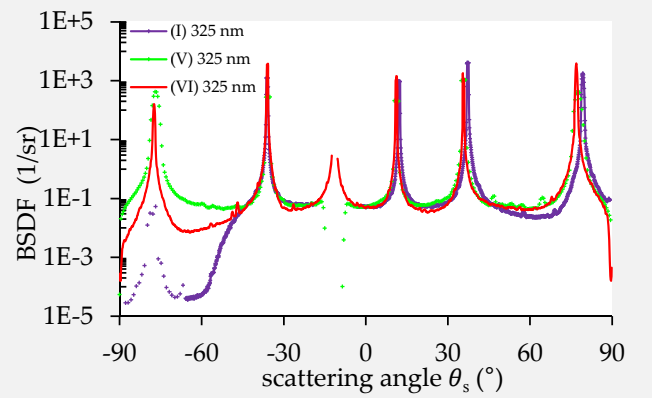

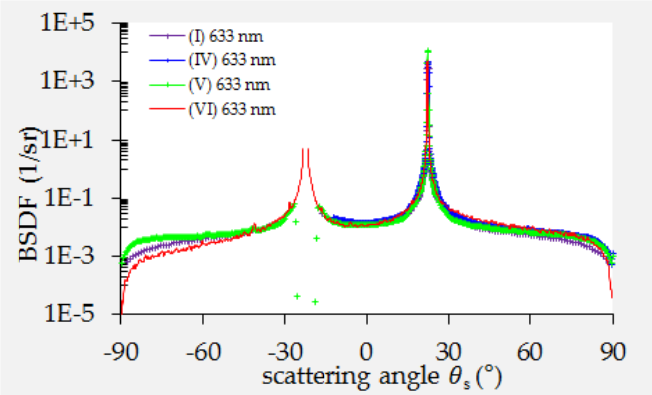

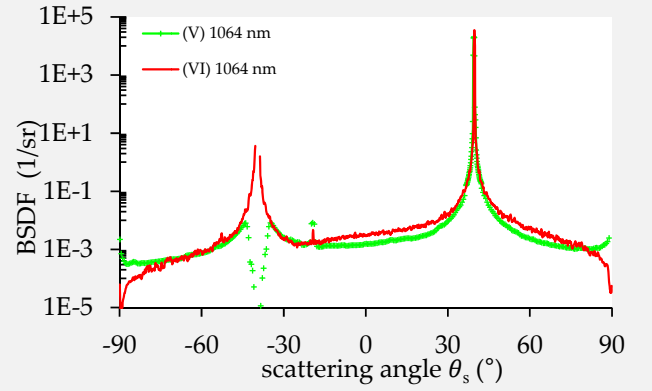

Fig. 23: RR measurements of the G# samples (holographic grating).

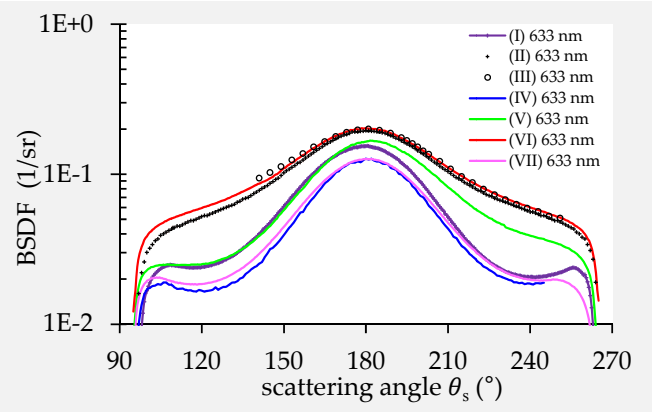

Fig. 24: RR measurements of the QVD sample (quasi volume diffusor).

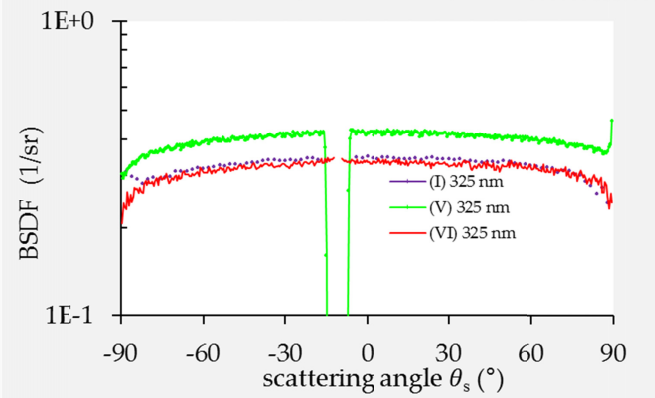

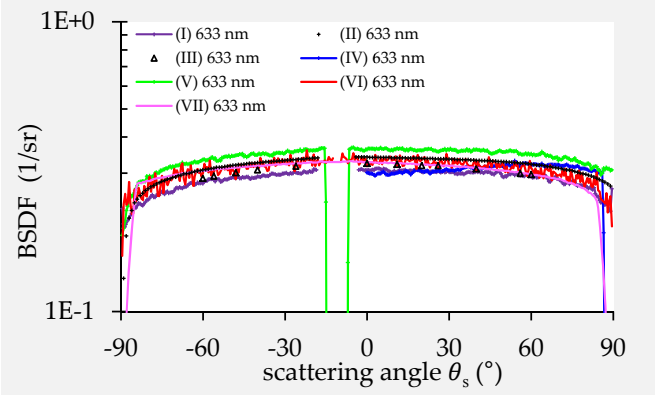

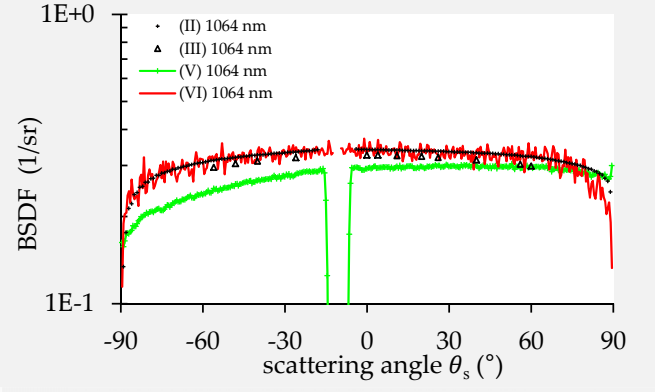

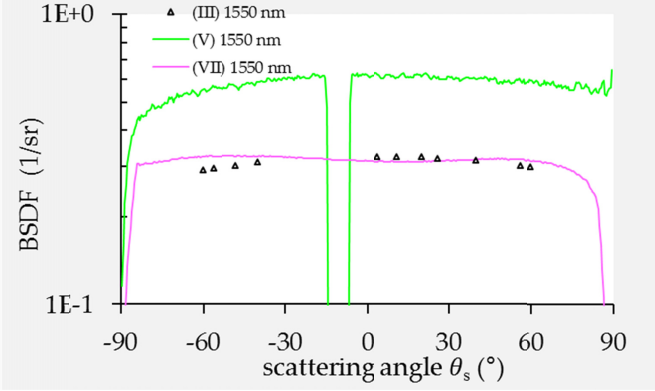

Fig. 25: RR measurements of the S# samples (white PTFE).

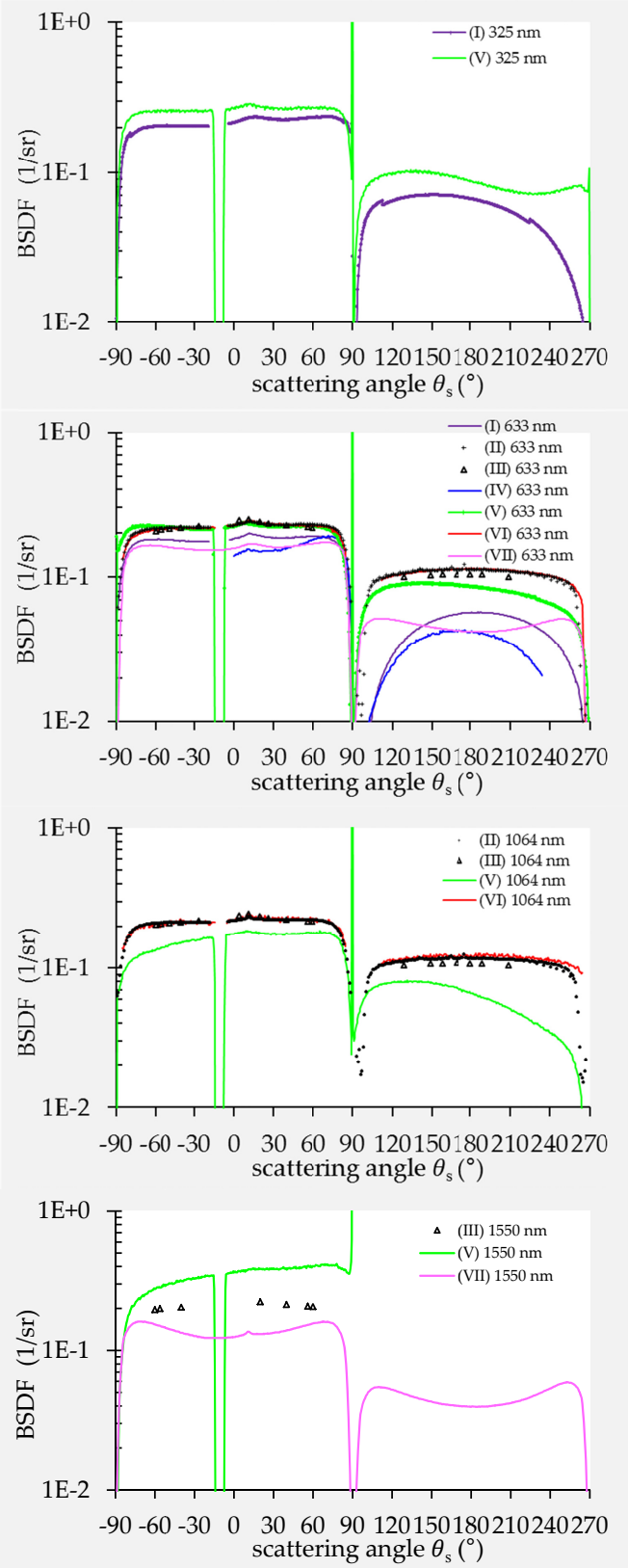

Fig. 26: RR measurements of the D# samples (fused silica volume diffusor).

Annex C

In this section, PSD functions are exemplary calculated from the BSDF measurements of participants V and VII (see Fig. 27). If the BSDF of the mirror samples are dominated by topographic scattering, the PSD functions should overlap. For PSD calculation the Rayleigh-Rice theory is used, which is valid for clean and smooth single surfaces. The PSDs of participant V fit well to the topography measurements on sample #M. The small deviations at large scattering angles are typical for dielectric protection layers [31]. The good overlap of the 1550 nm measurement, especially at small spatial frequencies, indicates that this measurement is sample representing.

That the PSDs of the scattering data of participant VII do not overlap indicates either a non-topographic scattering sample, or more probably, a calibration issue.

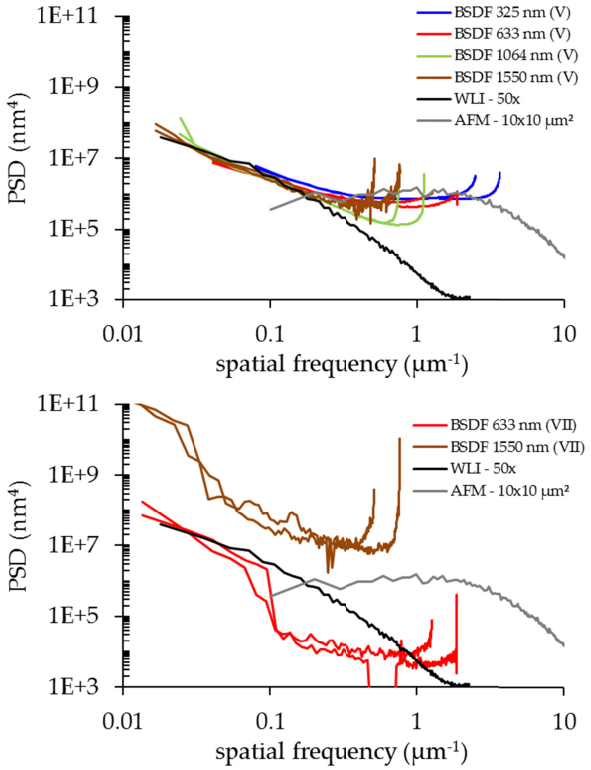

Fig. 27. Derived PSDs from participant V and VII compared to the topography measurements of the #M sample.

References

1. “Standard practice for goniometric optical scatter measurements,” ASTM E2387-05 (American Society for Testing and Materials, 2011).
2. ISO Working Draft ISO/WD 19986:2016(E), “Lasers and laser-related equipment — Test method for angle resolved scattering” (2016)
3. T. A. Leonard and P. Rudolph, "BRDF Round Robin Test of ASTM E1392," Proc. SPIE **1995**, 285–293 (1993).
4. U. S. Stefan Bäumer, Angela Duparré, Thomas Herrmann, "SLIOS - a contribution to standard procedures in stray light measurements," Proc. SPIE **3739**, 414–421 (1999).
5. ISO 13696, ‘Optics and Photonics – Lasers and Laser Related Equipment – Test Methods for Radiation Scattered by Optical Components’ (International Organization for Standardization, Geneva, Switzerland, 2002).
6. ASTM F 1048-87, ‘Standard Test Method for Measuring the Effective Surface Roughness of Optical Components by Total Integrated Scattering’ (American Society for Testing and Materials, Philadelphia, 1999)
7. P. Kadkhoda, A. Müller, D. Ristau, A. Duparré, S. Gliech, H. Lauth, U. Schuhmann, N. Reng, M. Tilsch, R. Schuhmann, C. Amra, C. Deumié, C. Jolie, H. Kessler, T. Lindström, C. G. Ribbing, and J. M. Bennett, "International round-robin experiment to test the International Organization for Standardization total-scattering draft standard.," Appl. Opt. **39**, 3321–32 (2000).
8. J. A. Detrio and S. M. Miner, "Standardized Total Integrated Scatter Measurements Of Optical Surfaces," Opt. Eng. **24**, 243419 (1985).
9. F. E. Nicodemus, J. C. Richmond, J. Hsia, I. W. Ginsberg, and T. Limperis, “Geometrical Considerations and Nomenclature for Reflectance,” NBS Monograph 160, 1–8 (1977).
10. J. C. Stover, S. Schröder, A. von Finck, D. Unglaub, and A. Duparré, "Estimating hemispherical scatter from incident plane measurements of isotropic samples scattering from both bulk and surface irregularities," **8838**, 883803-1–8 (2013).
11. S. Schröder, A. von Finck, A. Duparré, “Standardization of light scattering measurements,” Adv. Opt. Techn. 4(5-6) 361-375 (2015).
12. T. A. Germer, J. C. Stover, and S. Schröder, “Angle-resolved diffuse reflectance and transmittance,” in T. A. Germer, J. C. Zwinkels, and B. K. Tsai, *Experimental Methods in the Physical Sciences V46: Spectrophotometry: Accurate Measurement of Optical Properties of Materials,* eds. (Elsevier 2014), pp. 294-301.
13. P. Bousquet, F. Flory, and P. Roche, “Scattering from multi- layer thin films: theory and experiment,” J. Opt. Soc. Am. 71, 1115–1123 (1981).
14. J. M. Elson, J. P. Rahn, and J. M. Bennett, "Relationship of the total integrated scattering from multilayer-coated optics to angle of incidence, polarization, correlation length, and roughness cross-correlation properties," Appl. Opt. 22, 3207-3219 (1983)
15. C. Amra, "Light scattering from multilayer optics. II. Application to experiment," J. Opt. Soc. Am. A 11, 211-226 (1994)
16. M. Zerrad, S. Liukaityte, M. Lequime, and C. Amra, "Light scattered by optical coatings: numerical predictions and comparison to experiment for a global analysis," Appl. Opt. 55, 9680-9687 (2016)
17. AFM / WLI measurements and PSD calculations performed by Luisa Coriand and Nadja Felde (both Fraunhofer IOF).
18. P. Dumas, B. Bouffakhreddine, C. Amra, O. Vatel, E. Andre, R. Galindo, And F. Salvan, "Quantitative microroughness analysis down to the nanometer-scale," Europhysics Letters 22, 717-722 (1993).
19. A.Duparré, J.Ferre-Borrull,S. Gliech,G. Notni,J. Steinert, and J. Bennett, “Surface characterization techniques for determining the root-mean-square roughness and power spectral densities of optical components,” Appl. Opt. 41, 154–171 (2002).
20. T. Herffurth, S. Schröder, M. Trost, A. Duparré, and A. Tünnermann, “Comprehensive nanostructure and defect analysis using a simple 3D light-scatter sensor,” Appl. Opt. 52, 3279–3287 (2013).
21. S. Schröder, T. Herffurth, A. Duparré, and G. Notni, “Device and method for angularly resolved scattered light measurement,” Patent WO 002,010,127,872 (11 November 2010).
22. Harvey, J. E., “Light-scattering characteristics of optical surfaces” Ph.D. Dissertation, The University ofArizona, Tucson, Arizona (1979)
23. D. Hünerhoff, U. Grusemann, and A. Höpe, "New robot-based gonioreflectometer for measuring spectral diffuse reflection," Metrologia 43, S11–S16 (2006).
24. M. E. Nadal and P. Yvonne, "Near Infrared 45/0 Reflectance Factor of Pressed Polytetrafluoroethylene (PTFE) Powder," J. Res. Natl. Inst. Stand. Technol. 104, 185–188 (1999).
25. C.J. Chunnilall, et al. (2003). NPL scales for radiance factor and total diffuse reflectance. Metrologia 40.
26. JCGM 100:2008, “Evaluation of measurement data - Guide to the expression of uncertainty in measurement (GUM),” (2008).
27. A. Höpe, "Rotational radiance invariance of diffuse reflection standards," in NEWRAD 2005, 9th International Conference (2005).
28. B. McGuckin et. al., "Multiangle imaging spectroradiometer: optical characterization of the calibration panels," Appl. Opt. 36, (1997).
29. D. Haner et. al., "Polarization characteristics of Spectralon illuminated by coherent light," Appl. Opt. 38, 6350 (1999).
30. A. von Finck, Table top system for angle resolved light scattering measurement, Dissertation: TU Ilmenau, 2013.
31. A. von Finck, T. Herffurth, S. Schröder, A. Duparré, and S. Sinzinger, "Characterization of optical coatings using a multisource table-top scatterometer," Appl. Opt. **53**, A259–A269 (2014).